Nonlinear Observer-Based Control of Load Transitions in Homogeneous Charge Compression Ignition Engines

Chia-Jui Chiang, *Student Member, IEEE*, Anna G. Stefanopoulou, *Senior Member, IEEE*, and Mrdjan Janković, *Fellow, IEEE*

***Abstract*—This paper presents a model-based nonlinear feedback controller designed to regulate the crank angle at 50% fuel burned (θ_{CA50}) for a gasoline homogeneous charge compression ignition engine model during load transitions. The regulation of the combustion timing is based on manipulating the charge temperature through internal dilution, which is achieved by controlling the lift of a secondary opening of the exhaust valve, also known as the rebreathing lift. The nonlinear feedback controller developed is based on a positive semidefinite Lyapunov function using a simplified control model which contains only the cycle-to-cycle temperature dynamics. The nonlinear feedback controller depends on measurement of the combustion timing θ_{CA50} and estimation of the temperature at intake valve closing. Closed-loop simulation of the full-order engine model shows that the nonlinear feedback controller, along with a nonlinear observer, is able to regulate the combustion timing θ_{CA50} by stabilizing the temperature dynamics during load transitions. The closed-loop system with the observer-based feedback controller is shown to be robust to some classes of model uncertainty and measurement noise through simulation and an estimate of the region of attraction.**

***Index Terms*—Homogeneous charge compression ignition (HCCI) engines, nonlinear feedback control, nonlinear observer, positive semidefinite Lyapunov functions, stability.**

I. Introduction

HOMOGENEOUS charge compression ignition (HCCI) engines integrate the advantages of both spark ignition (SI) and compression ignition (CI) engines [1]: 1) high fuel efficiency resulting from high compression ratio and rapid heat release and 2) low NO_x and low particulate matter (PM) emissions due to low cylinder peak temperature (below 1700 K). Control of the HCCI engine, however, is difficult since its ignition cannot be directly actuated. The auto-ignition timing of HCCI combustion is determined by the cylinder charge conditions, rather than spark timing or fuel injection timing, which are used to initiate combustion in SI and CI engines, respectively, [2]. Instead, controlled auto-ignition requires regulation of the charge properties, especially temperature at the intake valve closing (IVC), as demonstrated by many experimental results [3], [4].

Manuscript received May 27, 2006; revised November 1, 2006; Manuscript received in final form January 29, 2007. Recommended by Associate Editor K. Fishbach. This work was supported in part by the National Science Foundation under Grant CMS-0201332 and by the Ford Motor Company under grants.

C.-J. Chiang and A. G. Stefanopoulou are with the Department of Mechanical Engineering, University of Michigan, Ann Arbor, MI 48109 USA (e-mail cjchiang@umich.edu; annastef@umich.edu).

M. Janković is with the Ford Research and Advanced Engineering Laboratory, Dearborn, MI 48121 USA (e-mail: mjankov1@ford.com).

Color versions of Figs. 1–3 and 5–12 are available online at http://ieeexplore.ieee.org.

Digital Object Identifier 10.1109/TCST.2007.894637

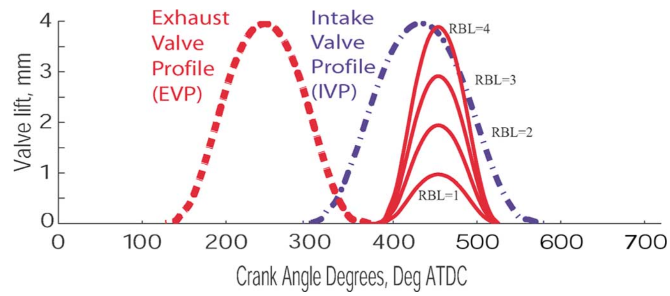

Fig. 1. Exhaust, intake, and rebreathing valve profiles.

Charge temperature is the primary mechanism for controlling ignition timing in an HCCI engine, especially when exhaust gas recirculation (EGR) is used [3]–[5]. The recirculation of hot exhaust gas provides high dilution and also changes the charge temperature inside the cylinder [2], [6]. One attractive way to recirculate the hot exhaust gas involves a secondary opening of the exhaust valve during the intake stroke (rebreathing), which we refer to as the rebreathing lift (RBL), as shown in the valve profiles in Fig. 1. This actuation provides high dilution levels from the exhaust gas heat, which can increase the charge temperature for the next cycle and thus determines the ignition and the exhaust temperature of the subsequent cycle [7], [8].

In previous work, regulation of the combustion timing in HCCI engines has been successfully achieved via linear control techniques based on linearized models [9]–[11]. Although successful in controlling timing as shown by simulation and experiments, linear controllers do not address the stability issue associated with the nonlinear behavior shown in [12]. The nonlinearity in the temperature dynamics introduces multiple equilibria as shown in [12] and, thus, raises concerns on the stability of linear controllers during large disturbances. Therefore, unlike previous work, we design a nonlinear feedback controller based on the mean value model (MVM) in [7], that takes into account the nonlinear temperature dynamics. The control objective is to regulate crank angle, where 50% of the fuel is burned (θ_{CA50}) by changing RBL during fuel step changes at constant engine speed.

It has been shown in [12] that the charge temperature at IVC, $T_{\rm ivc}$, and the exhaust runner temperature, $T_{\rm er}$, are the two cycle-to-cycle interacting temperature dynamics in an HCCI engine with high dilution from the exhaust. In order to control the combustion timing, it is necessary to stabilize the temperature dynamics. Based on the MVM in [7], we illustrate transitions between temperature equilibria during critical load transitions. We demonstrate that nonoptimized sequences of the input command RBL from a static feedforward controller can result in large temperature excursion that can damage the engine or lead to misfire. On the other hand, a linear feedback controller in [9] was able to produce commands that safely allow load transition between two stable equilibria and regulation of the combustion timing. The nonlinear feedback controller designed here stabilizes the temperature dynamics even during large fuel step changes by utilizing the combustion timing θ_{CA50} measurement.

In Section II, we summarize the HCCI engine model in [7] which includes manifold filling dynamics and a combustion model. In Section III, we design a nonlinear controller based on a simplified model to regulate the combustion timing θ_{CA50} by stabilizing the temperature dynamics during fuel step changes. In Section III-A, a simplified model which contains only the cycle-to-cycle temperature dynamics is constructed based on the full-order model in [7]. In Section III-B, a nonlinear controller is developed based on a positive semidefinite Lyapunov function using the simple model from Section III-A. In Section IV, we present an estimate of the region of attraction of the closed-loop system with the nonlinear controller designed in Section III-B. In Section V, we design a nonlinear observer for the temperature at IVC $T_{\rm ivc}$ by linearization of the error dynamics using output injection. In Section VI, we show closed-loop simulations with the controller designed in Section III-B and the observer designed in Section V using a noisy θ_{CA50} measurement and model uncertainties associated to the full-order model in [7]. We also compare the performance of the observer-based feedback controller with a static feedforward controller during critical load transitions. It is shown through simulation that the closed-loop system is robust to model uncertainties such as the manifold filling dynamics, exhaust runner heat transfer, the cycle-to-cycle variation of θ_{CA50} and the uncertainty in the nonlinearity of the temperature dynamics.

II. HCCI Engine Model

The model we use in this control study is based on the mean value model (MVM) constructed in [7], where the cylinder is modeled as a pump based on cycle-average cylinder flows under constant engine speed. Fig. 2 shows the schematic diagram associated with the engine model. This engine model includes three relevant volumes: 1) the intake manifold denoted by subscript 1; 2) the exhaust manifold denoted by subscript 2; and 3) the cylinder denoted by subscript c. The atmospheric conditions are denoted with subscript 0. For each volume, the volumes are denoted by V, pressures by p, temperatures by T, and masses by m. The rate of the flow from volume x to volume y is denoted by W_{xy} and is calculated using the orifice flow equation [13,

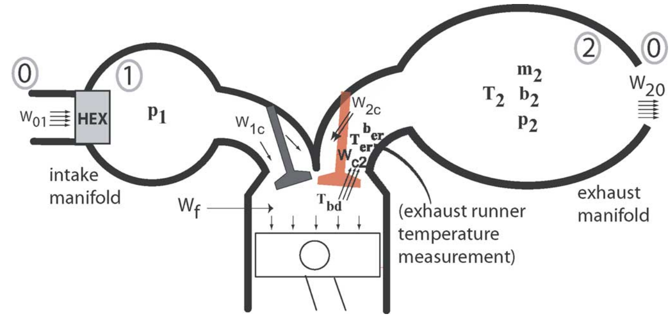

Fig. 2. Schematic diagram of the engine.

App. C]. A heat exchanger (HEX) maintains the intake manifold at isothermal conditions, $T_1 = 90\,^\circ$C (363 K). The mean value model in [7] includes seven states: one state in the intake manifold, pressure p_1; three states in the exhaust manifold, mass m_2, burned gas fraction b_2 and pressure p_2; three states from the unit delay between the intake and exhaust processes, the average mass flow rate from the cylinder to the exhaust manifold W_{c2}, the burned gas fraction and temperature of the gas in the exhaust runner $b_{\rm er}$ and $T_{\rm er}$. This model has been validated with experimental data in [7]. All the model equations can be found in the Appendix and details are available in [7].

III. Control Development

We first construct a simplified discrete-time model and then design a nonlinear feedback controller to regulate the combustion timing by stabilizing the temperature dynamics during fuel step changes. A list of all the parameters used in the model and controller can be found in Table I.

A. Simplified Control Model

In this section, we construct a simple discrete-time model for control development based on the MVM in [7]. This simplified model contains only the cycle-to-cycle temperature dynamics that is critical to the system stability as suggested in [12]. First, neglecting the difference in heat capacities and burned gas left in the cylinder, the charge temperature at IVC is approximated as the weighted temperature of the mixing mass flow rate from the intake manifold $(W_{1c}T_1)$ and the rebreathed flow $(W_{2c}T_{\rm er})$

$$T_{\rm ivc} = \frac{W_{2c}T_{\rm er} + W_{1c}T_1}{W_{2c} + W_{1c}}. \quad (1)$$

By defining $x_r = (W_{2c})/(W_{2c} + W_{1c})$ as the residual gas fraction, (1) can be rewritten as

$$T_{\rm ivc}(k) = x_r(k)T_{\rm er}(k) + (1 - x_r(k))\,T_1 \quad (2)$$

for temperature at IVC of the kth cycle. The residual gas fraction x_r is a function of RBL only by assuming limited variation in the manifold pressures. This assumption is motivated by the fact that the HCCI engine will typically operate under unthrottled conditions. Fig. 3 shows the effect of RBL on the residual fraction x_r as predicted by the full-order model in [7] and summarized in the Appendix. As RBL increases, more residual gas is brought back into the cylinder, resulting in higher x_r.

TABLE I
LIST OF ALL PARAMETERS AND THEIR VALUES, IF CONSTANT

	Definition	Value
α	RBL exponent in W_{2c}	0.5794
β_0	constant term of p_{ivc}, kPa	1.035
β_1	linear term of p_{ivc} dependence on p_1	1.1568
$\Delta\theta$	burn duration	
γ	ratio of specific heats	1.40
κ_0	constant term of W_{2c}	0.5729
κ_1	modulation of W_{2c} by $\frac{p_1}{p_2}$	-0.52039
θ_c	location of instantaneous heat release	
θ_{CA50}	location of 50% fuel burned	
θ_{soc}	location of start of combustion	
τ	engine cycle period, sec	0.12
A	scaling constant for the Arrhenius integral	0.4167
A_2	heat transfer area in the exh manifold, m^2	0.3149
A_{er}	heat transfer area in the exh runner, m^2	
AFR_c	air-to-fuel ratio in cylinder	
b_0	constant term in e parametrization	0.4086
b_1	linear term in e dependence on θ_{soc}	-0.0839
b_2	square term in e dependence on θ_{soc}	-0.0153
b_{bd}	burned gas fraction of blowdown gas	
b_{er}	burned gas fraction in exhaust runner	
b_c	burned gas fraction in cylinder at IVC	
b_2	burned gas fraction in exh manifold	
c_L	nonlinear feedback control gain	0.8
C_p	constant pressure specific heat, J/kg-K	1036.9
C_v	constant volume specific heat, J/kg-K	740.625
D_{er}	diameter of the exhaust runner, m	0.035
e	burn duration averaging parameter	
E_a	Arrhenius activation energy, J/kg	1831930
E_c	combustion reaction activation energy, J/mol	185000
h_2	exh manifold heat transfer coeff, W/m^2-K	267
h_{er}	exh runner heat transfer coeff, W/m^2-K	84
k	burn duration parameter	0.5397
K_I	integral control gain, K	5
m_c	total mass in cylinder, kg	
m_f	mass of the fuel injected per cycle	
m_x	mass of gas in volume x	
n	Arrhenius reaction's sensitivity to pressure	1.367
n_c	polytropic constant during compression	1.30
n_e	polytropic constant during expansion	1.35
p_x	pressure in volume x	
p_{bc}	pressure in cylinder before heat release	
p_{ac}	pressure in cylinder after heat release	
p_{ivc}	pressure in cylinder at intake valve closing	
q	integral state	
Q_{LHV}	lower heating value of gasoline, kJ/kg	44000
R	gas constant, J/kg-K	296.25
R_u	universal gas constant, J/mol-K	8.314
RBL	rebreathing valve lift actuation signal, *mm*	
t_r	EVC to middle of intake stroke, sec	0.015
T_{ac}	temp in cylinder after heat release, K	
T_{bc}	temp in cylinder before heat release, K	
T_{er}	exhaust runner temperature, K	
T_{ivc}	temp in cylinder at intake valve closing, K	
T_m	mean temp during the combustion, K	
T_w	wall (ambient) temperature, K	400
T_x	temperature in volume x, K	
V_1	intake manifold volume, m^3	0.0013
V_2	exhaust manifold volume, m^3	0.015
V_L	Lyapunov function	
W_{xy}	mass flow rate from volume x to y, kg/s	
W_f	fuel flow rate, kg/s	
x_r	residual gas fraction in cylinder	

The reinducted product temperature, $T_{\rm er}$, which is assumed to be the measured temperature in the exhaust runner, can be calculated from the temperature of the blowdown gas in the previous cycle with a factor 0.9 to account for the heat transfer in the exhaust runner

$$T_{\rm er}(k) = 0.9 T_{\rm bd}(k-1). \tag{3}$$

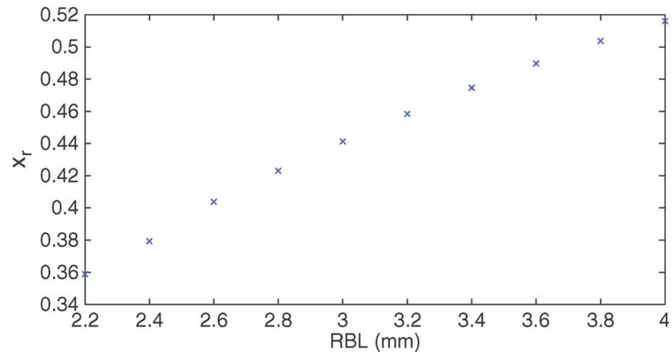

Fig. 3. Effect of RBL on residual gas fraction.

Note that this is a simplification of the seventh state (45) in the Appendix that represents more accurately the heat lost in the exhaust runner. The blowdown temperature $T_{\rm bd}$ is derived by tracing the temperature variations during compression, combustion, expansion, and blowdown process in [7]

$$T_{\rm bd}(k) = T_{\rm ivc}(k)\left(\frac{p_2}{p_{\rm ivc}}\right)^{1-\frac{1}{n_e}} \times \left[\left(\frac{V_c(\theta_c)}{V_{\rm ivc}}\right)^{n_e-n_c} + \frac{V_c^{n_e-1}(\theta_c) R Q_{\rm LHV} m_f}{C_v V_{\rm ivc}^{n_e} p_{\rm ivc}}\right]^{\frac{1}{n_e}} \tag{4}$$

where m_f is the amount of fuel injected per cycle, $Q_{\rm LHV}$ is the lower heating value of the fuel, R is the gas constant, C_v is the specific heat at constant volume, n_c and n_e are the polytropic constants during compression and expansion, respectively, $V_{\rm ivc}$ is the cylinder volume at IVC and $V_c(\theta_c)$ denotes the cylinder volume at θ_c, the end of combustion, which is calculated from the start of combustion $\theta_{\rm soc}$ and combustion duration $\Delta\theta$

$$\theta_c = \theta_{\rm soc} + \Delta\theta. \tag{5}$$

The start of combustion $\theta_{\rm soc}$ is determined mainly by the charge temperature [5], as can be observed from the Arrhenius integral [14]

$$\int_{\theta_{\rm ivc}}^{\theta_{\rm soc}} A p_{\rm ivc}^{n} v_{\rm ivc}^{n_c n}(\vartheta) \exp\left(-\frac{E_a v_{\rm ivc}^{1-n_c}(\vartheta)}{R T_{\rm ivc}}\right) d\vartheta = 1$$
$$v_{\rm ivc}(\vartheta) = V_{\rm ivc}/V_c(\vartheta) \tag{6}$$

where A is a scaling constant, E_a is the Arrhenius activation energy, n indicates the reaction's sensitivity to pressure, and $v_{\rm ivc}$ is the cylinder volume ratio. On the other hand, the combustion duration $\Delta\theta$ in (5) can be calculated by the burning velocity theory [5], [7], [15], which is originally derived for laminar burning, with adapted coefficients k and e capturing the combustion efficiency and heat transfer inside the cylinder

$$\begin{aligned}\Delta\theta &= k (T_{\rm soc})^{(-2/3)} (T_m)^{1/3} \exp\left(\frac{E_c}{3 R_u T_m}\right)\\ T_m &= T_{\rm soc} + e\Delta T\\ \Delta T &= \frac{Q_{\rm LHV} m_f}{C_v m_c}\\ e &= b_0 + b_1\theta_{\rm soc} + b_2\theta_{\rm soc}^2\end{aligned} \tag{7}$$

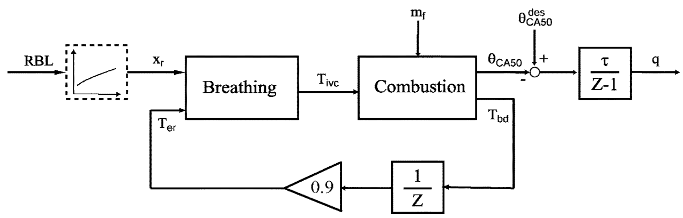

Fig. 4. Block diagram of the simplified control model.

where E_c is the activation energy for combustion reaction, R_u is the universal gas constant, and T_m is the mean temperature during the combustion process. Combining (4)–(7), the combustion model gives $T_{\rm bd}$ as a function of $T_{\rm ivc}$ and m_f

$$T_{\rm bd}(k) = f_c\left(T_{\rm ivc}(k), m_f(k)\right). \tag{8}$$

In this control model, temperature $T_{\rm ivc}$ is picked as the discrete state, residual fraction x_r acts as the control input, and fuel m_f is the measurable disturbance. Thus, by combining (2), (3), and (8), the state equation can be summarized as

$$T_{\rm ivc}(k+1) = \left[0.9 f_c\left(T_{\rm ivc}(k), m_f(k)\right) - T_1\right] x_r(k+1) + T_1. \tag{9}$$

The simplified control model is summarized as the block diagram in Fig. 4 with one integral state q added for asymptotic regulation of the θ_{CA50} set-point

$$q(k+1) = q(k) + \tau\left(\theta_{CA50}^{\rm des} - \theta_{CA50}(k)\right). \tag{10}$$

For the controller design and gain tuning in Section III-B, the performance output crank angle where 50% of the fuel is burned θ_{CA50} is approximated by $\widetilde{\theta}_{CA50}$ in (11) as a linear function of the state $T_{\rm ivc}$ around the desired operating $\theta_{CA50} = 5^\circ$ after top dead center (ATDC) at different fueling level m_f

$$\widetilde{\theta}_{CA50} = g_0(m_f) + g_1(m_f) T_{\rm ivc}. \tag{11}$$

Fig. 5 shows the linear approximation (dashed lines) of the nonmonotonic function of θ_{CA50} versus $T_{\rm ivc}$ as predicted by the full-order model in [7] and (56)–(64).

For the estimate of the attraction region in Section IV and the observer design in Section V, a more accurate approximation of θ_{CA50} is used to account for the nonlinearity governed by (56)–(64) and observed in Fig. 5

$$\overline{\theta}_{CA50} = h_0(m_f) + h_1(m_f) T_{\rm ivc} + h_2(m_f) T_{\rm ivc}^2. \tag{12}$$

B. Nonlinear Feedback Controller Design

To regulate the combustion timing by stabilizing the temperature dynamics during fuel step changes, a nonlinear feedback controller is designed based on the theorem in [16] for a positive semidefinite Lyapunov function in a discrete system. The main advantage is a reduction in the complexity of the candidate Lyapunov function that often occurs in concrete examples when the positive definite requirement is weakened to semidefinite [16]–[18]. A candidate Lyapunov function with parameter

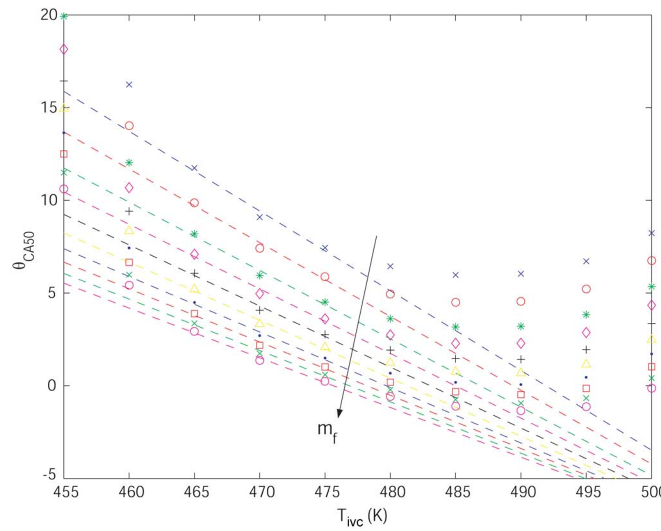

Fig. 5. Crank angle where 50% of fuel is burned in degrees ATDC as a function of $T_{\rm ivc}$ in Kelvin.

K_I is chosen to force the integral state q to be bounded relative to the state $T_{\rm ivc}$

$$V_L(k) = V^2(k) = \left(K_I q(k) + T_{\rm ivc}(k)\right)^2. \tag{13}$$

Thus, if it can later be proven that any one of $T_{\rm ivc}$ or q is bounded, then both of them are. The difference equation of the Lyapunov function V_L is given by

$$V_L(k+1) - V_L(k) = \left(V(k+1) + V(k)\right)\left(V(k+1) - V(k)\right) \tag{14}$$

where

$$\begin{aligned} V(k+1) - V(k) = & K_I \tau\left[\theta_{CA50}^{\rm des} - g_0(m_f(k)) - g_1(m_f(k))\, T_{\rm ivc}(k)\right] \\ & + \left[0.9 f_c\left(T_{\rm ivc}(k), m_f(k)\right) - T_1\right] x_r(k+1) \\ & - T_{\rm ivc}(k) + T_1. \end{aligned} \tag{15}$$

To render the difference of the Lyapunov function V_L negative semidefinite for the application of the theorem in [16], the choice of the control law with appropriate gain c_L

$$\begin{aligned} x_r(k+1) = & \left[-K_I \tau\left(\theta_{CA50}^{\rm des} - g_0\left(m_f(k)\right) - g_1\left(m_f(k)\right) T_{\rm ivc}(k)\right)\right. \\ & \left. - c_L V(k) + T_{\rm ivc}(k) - T_1\right] / \\ & \left[0.9 f_c\left(T_{\rm ivc}(k), m_f(k)\right) - T_1\right] \end{aligned} \tag{16}$$

results in

$$V(k+1) - V(k) = -c_L V(k) \tag{17}$$

and

$$V(k+1) + V(k) = (2 - c_L) V(k) \tag{18}$$

and, thus, renders the difference equation of the Lyapunov function V_L negative semidefinite for $0 < c_L < 2$

$$V_L(k+1) - V_L(k) = -c_L(2 - c_L) V^2(k). \tag{19}$$

Note that the denominator of the control (16), $0.9f_c(T_{\rm ivc}(k), m_f(k)) - T_1$, is always greater than zero since the exhaust runner temperature $T_{\rm er}$ in (3) is always higher than the intake manifold temperature T_1. The goal now is to understand what (19) implies regarding the stability of the model (9) and (10) in Section III-A. Based on the theorem in [16], for a positive semidefinite Lyapunov function V_L in a time-invariant discrete system with $\Delta V_L \leq 0$, the equilibrium point is stable in the sense of Lyapunov if it is asymptotically stable for all the perturbed initial conditions $x_0 \in Z$, where Z is the largest invariant set in $\{x | V_L(x) = 0\}$. Thus, to prove the stability of the closed-loop system, we first need to show that it is asymptotically stable when V_L is set to zero. With $V_L = 0$, the control signal in (16) becomes

$$x_r(k+1) \to \big[-K_I\tau\big(\theta_{CA50}^{\rm des} - g_0(m_f(k)) - g_1(m_f(k))\,T_{\rm ivc}(k)\big) + T_{\rm ivc}(k) - T_1\big]/[0.9f_c\,(T_{\rm ivc}(k), m_f(k)) - T_1]\,. \tag{20}$$

Applying the control (20) to the state (9) cancels the nonlinear term $0.9f_c(T_{\rm ivc}(k), m_f(k)) - T_1$ in (9), resulting in a linear state equation

$$T_{\rm ivc}(k+1) = (1 + K_I\tau g_1\,(m_f(k)))\,T_{\rm ivc}(k) + K_I\tau\,\big(g_0\,(m_f(k)) - \theta_{CA50}^{\rm des}\big) \tag{21}$$

which is asymptotically stable if

$$|1 + K_I\tau g_1\,(m_f(k))| < 1. \tag{22}$$

Note here that the stability condition involves the integral gain K_I and the slope of the approximated $\widetilde{\theta}_{CA50}$ in (11) and Fig. 5. Under this condition, the states $T_{\rm ivc}$ and q of (9) and (10) are asymptotically stable conditionally to the largest positively invariant set contained in $Z = \{T_{\rm ivc} | V_L = 0\}$. According to the theorem in [16], the states $T_{\rm ivc}$ and q are bounded, and thus, by Lasalle's theorem [19], they approach the largest positively invariant set contained in $W = \{T_{\rm ivc} | \Delta V_L = 0\}$. However, from (13) and (19), $W = Z$. Thus, it follows that the control signal (16) converges to (20), and consequently, the states converge to a constant value, i.e., an equilibrium point. This then gives that the steady state θ_{CA50} error is zero. Combining (13) and (16), we can summarize the designed nonlinear controller as

$$x_r(k+1) = \big[(1 - c_L + K_I\tau g_1(m_f(k)))T_{\rm ivc}(k) - c_LK_Iq(k) - T_1 - K_I\tau \times \big(\theta_{CA50}^{\rm des} - g_0(m_f(k))\big)\big]/ [0.9f_c(T_{\rm ivc}(k), m_f(k)) - T_1]\,. \tag{23}$$

Note that to implement the controller (23), information from the previous cycle is needed. Specifically, the θ_{CA50} measurement in the previous cycle is used to calculate the integral state q with (10) and to estimate the state $T_{\rm ivc}$ in the previous cycle by the nonlinear observer designed in Section V.

IV. Estimate of the Region of Attraction

The controller (23) is established to achieve local asymptotic stability in response to the linear approximation of $\widetilde{\theta}_{CA50}$ in (11). The simulation results in Section VI provide additional assurance that the nonlinear controller is robust to model uncertainty and measurement noise. However, it is almost impossible to take into account all the uncertainties in the model. Hence, it is of interest to find the region of attraction of the desired operating points, or at least an estimate of it. This section is devoted to assessing the region of attraction for the equilibrium point to examine the robustness of the closed-loop system with the controller designed in Section III-B. The technique for the estimate of the region of attraction [20] is applied to the discrete-time closed-loop system. First, by substituting the control (23) into (9) and the output (12) into (10), the closed-loop system becomes

$$\begin{aligned} T_{\rm ivc}(k+1) &= (1 - c_L + K_I\tau g_1\,(m_f(k)))\,T_{\rm ivc}(k) - c_LK_Iq(k) - K_I\tau\,\big(\theta_{CA50}^{\rm des} - g_0\,(m_f(k))\big) \\ q(k+1) &= q(k) + \tau\,\big[\theta_{CA50}^{\rm des} - h_0\,(m_f(k)) - h_1\,(m_f(k))\,T_{\rm ivc}(k) - h_2\,(m_f(k))\,T_{\rm ivc}^2(k)\big]\,. \end{aligned} \tag{24}$$

By centering the equilibrium around the origin, the closed-loop state (24) can then be transformed to

$$\begin{aligned} \delta T_{\rm ivc}(k+1) &= (1 - c_L + K_I\tau g_1(m_f(k)))\delta T_{\rm ivc}(k) - c_LK_I\delta q(k) \\ \delta q(k+1) &= \delta q(k) - \tau h_2\,(m_f(k))\,\delta T_{\rm ivc}^2(k) + \tau\sqrt{h_1^2(m_f(k)) - 4h_2(m_f(k))\big(h_0(m_f(k)) - \theta_{CA50}^{\rm des}\big)} \times \delta T_{\rm ivc}(k) \end{aligned} \tag{25}$$

which can be written as

$$x(k+1) = Ax(k) + \Delta f\,(x(k)) \tag{26}$$

where (27), holds at the bottom of the page, and the matrix A is Hurwitz for all the desired operating points at different fueling levels. Let

$$V_A(k) = x^T(k)Px(k) \tag{28}$$

$$\begin{aligned} x(k) &= [\delta T_{\rm ivc}(k) \quad \delta q(k)]^T \\ A &= \begin{bmatrix} 1 - c_L + K_I\tau g_1\,(m_f(k)) & -c_LK_I \\ \tau\sqrt{h_1^2\,(m_f(k)) - 4h_2\,(m_f(k))\,\big(h_0\,(m_f(k)) - \theta_{CA50}^{\rm des}\big)} & 1 \end{bmatrix} \\ \Delta f\,(x(k)) &= \big[0 \quad -\tau h_2\,(m_f(k))\,\delta T_{\rm ivc}^2(k)\big]^T \end{aligned} \tag{27}$$

be a Lyapunov function for the system (26) in a certain neighborhood of the origin. The positive definite real symmetric matrix P is a unique solution of the discrete-time Lyapunov equation

$$A^T PA - P + Q = 0 \tag{29}$$

with a positive definite or positive semidefinite real symmetric choice of Q. For the present system in (26), δT_{ivc} identically zero implies that δq is identically zero. Thus, instead of choosing a positive definite Q, we could choose Q to be a positive semidefinite matrix [21], such as

$$Q = \begin{bmatrix} 1 & 0 \\ 0 & 0 \end{bmatrix}. \tag{30}$$

Since our interest here is in estimating the region of attraction, we need to determine a domain D about the origin, where $\Delta V_A(k) = V_A(k+1) - V_A(k)$ is negative definite and a constant $c > 0$, such that $\Omega_c = \{x | V_A(x) \leq c\}$ is a subset of D. We are interested in the largest set Ω_c that we can determine, that is, the largest value for the constant c. Notice that we do not have to worry about checking positive definiteness of $V_A(x)$ in D because $V_A(x)$ is positive definite for all x. Moreover, $V_A(x)$ is radially unbounded; hence, Ω_c is bounded for any $c > 0$. The difference of the Lyapunov function $V_A(k)$ in (28) along the trajectories of the system (26) is given by

$$\begin{aligned} \Delta V_A(k) =& -x^T(k)Qx(k) + 2x^T A^T P \Delta f(x(k)) \\ &+ \Delta f^T(x(k)) P \Delta f(x(k)) \\ =& -\delta T_{\text{ivc}}^2 \left[1 + a_0(m_f(k))\delta q + a_1(m_f(k))\delta T_{\text{ivc}} \right. \\ &\left. + a_2(m_f(k))\delta T_{\text{ivc}}^2\right]. \end{aligned} \tag{31}$$

Thus, $\Delta V_A(k)$ is negative definite when

$$1 + a_0(m_f(k))\delta q + a_1(m_f(k))\delta T_{\text{ivc}} + a_2(m_f(k))\delta T_{\text{ivc}}^2 > 0. \tag{32}$$

The parameters a_0, a_1, and a_2 are functions of fueling level only, given fixed c_L and K_I. Thus, the domain D, where $\Delta V_A(k)$ is negative definite can be found by solving (32) for each fueling level. For each fueling level, the region of attraction Ω_c can then be estimated by plotting the contour of $V_A(x) = x^T Px = c$ for increasing values of c until we determine the largest c for which $V_A(x) = c$ will be in $D = \{x | \Delta V_A(x) < 0\}$. The resulting contours of $\Delta V_A(x) = 0$ and region of attraction Ω_c at fueling level 9 and 16 mg are shown in Fig. 12 in Section VI.

V. Nonlinear Observer Design

Since the temperature at IVC T_{ivc} cannot be measured, an observer is required in order to implement the feedback control (23). The specific observer is designed based on the method detailed in [22] for linearizable error dynamics. By approximating the function $f_c(T_{\text{ivc}}(k), m_f(k))$ as a quadratic polynomial of the state T_{ivc} at different fueling levels m_f, the state equation in (9) can be rewritten as

$$\begin{aligned} T_{\text{ivc}}(k+1) =& \left[l_0(m_f) + l_1(m_f)T_{\text{ivc}}(k)\right. \\ &\left. + l_2(m_f)T_{\text{ivc}}^2(k)\right] x_r(k+1) + T_1. \end{aligned} \tag{33}$$

To linearize the state equation via output injection, the nonlinear term T_{ivc}^2 can be derived from the output equation in (12) as

$$T_{\text{ivc}}^2 = \frac{\overline{\theta}_{CA50} - h_0(m_f) - h_1(m_f)T_{\text{ivc}}}{h_2(m_f)}. \tag{34}$$

By substituting (34) into (33), a linearized state equation with output injection is obtained

$$\begin{aligned} T_{\text{ivc}}(k+1) =& \gamma_1(m_f)x_r(k+1)T_{\text{ivc}}(k) \\ &+ \gamma_2(m_f)x_r(k+1)\overline{\theta}_{CA50} + \gamma_0(m_f)x_r(k+1) + T_1 \end{aligned} \tag{35}$$

where $\gamma_0 = l_0 - h_0 l_2/h_2$, $\gamma_1 = l_1 - h_1 l_2/h_2$, and $\gamma_2 = l_2/h_2$ are functions of fueling level only. The observer is then designed as

$$\begin{aligned} \widehat{T}_{\text{ivc}}(k+1) =& \gamma_1(m_f)x_r(k+1)\widehat{T}_{\text{ivc}}(k) \\ &+ \gamma_2(m_f)x_r(k+1)\overline{\theta}_{CA50} + \gamma_0(m_f)x_r(k+1) + T_1. \end{aligned} \tag{36}$$

Under the previous construction, the error dynamics $e(k) = T_{\text{ivc}}(k) - \widehat{T}_{\text{ivc}}(k)$ become linear

$$e(k+1) = \gamma_1(m_f)x_r(k+1)e(k) \tag{37}$$

and for all the applicable fueling levels m_f and RBL (or x_r) in our study, $|\gamma_1(m_f)x_r(\text{RBL})| < 1$. Thus, the error $e \to 0$ exponentially. Note that, however, the stability of the resulting observer-based closed-loop system is not guaranteed. Stability is examined via simulation along with the performance of the controller in Section VI.

VI. Control Results

In this section, we first apply the state feedback controller (23) to the full-order model modified from the model in [7], which includes the manifold filling dynamics (39)–(44), a more accurate heat transfer model (45) and the process from IVC to blowdown (46)–(64). We then examine the performance of the controller (23) along with the observer (36). To emulate the cycle-to-cycle variation observed in the experiment data [9], a Gaussian distributed noise with standard deviation 1° is added to the θ_{CA50} measurement. The sample time τ of the integrator is equal to the engine cycle time 0.12 s (1000 r/min). The parameter c_L needs to satisfy $0 < c_L < 2$ and K_I is chosen to satisfy (22) for the slope g_1 in Fig. 11 for all the fueling levels m_f at which an HCCI engine operates. We choose $c_L = 0.8$ and $K_I = 5$ K so that the eigenvalues of the matrix A in the closed-loop system (26) stay within the right half plane of the unit circle to achieve stability and avoid ringing. Fig. 6 shows the controlled performance with the state feedback controller (23) during fuel steps 9–11–9 mg/cycle. The nonlinear state feedback controller stabilizes the temperature T_{ivc} and regulates the combustion timing during fuel steps. The integral state q is bounded in relation to the temperature T_{ivc}, resulting from the construction of the Lyapunov function V_L in (13).

Next, we show the closed-loop performance when the nonlinear feedback controller (23) is augmented with the observer (36) for the state T_{ivc}. The closed-loop dynamics with the observer-based feedback controller is compared with the dynamics associated with a static feedforward controller $x_r(k) = f_{ff}(m_f(k))$, which is easy to implement with a lookup table since the fueling level is known. The feedforward map $f_{ff}(\cdot)$

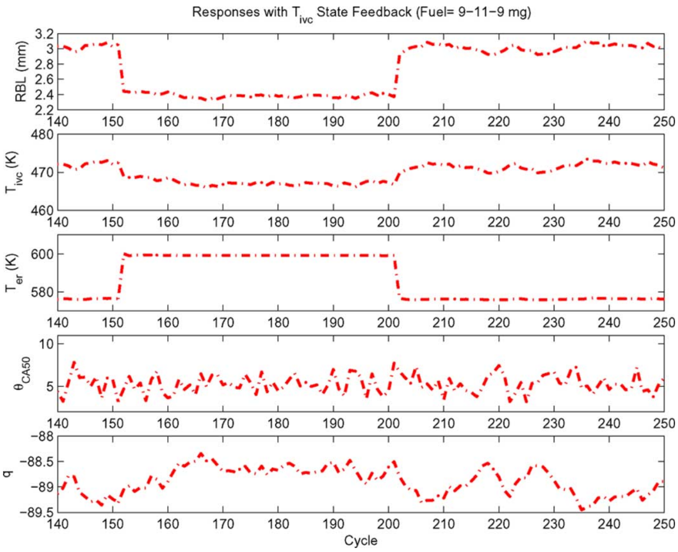

Fig. 6. Controlled responses with the full-state feedback during fuel steps 9–11–9 mg/cycle.

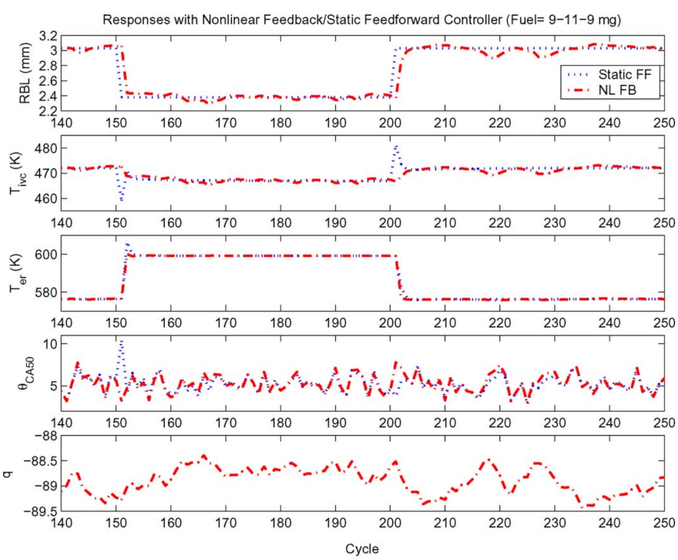

Fig. 7. Controlled responses with the observer-based feedback controller and a static feedforward controller during fuel steps 9–11–9 mg/cycle. The observer-based feedback controller does a much better job regulating the combustion timing during transient.

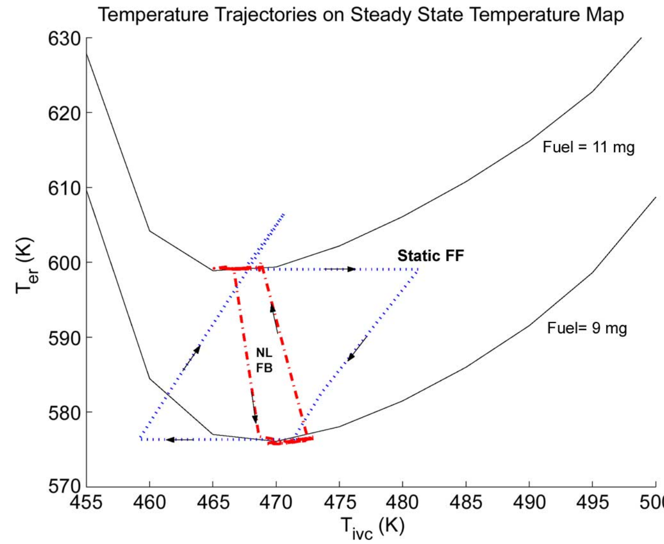

Fig. 8. Controlled temperature trajectories with the observer-based feedback controller and a static feedforward controller during fuel steps 9–11–9 mg/cycle. Both controllers are able to regulate the steady-state IVC temperature $T_{\rm ivc}$ to the optimum equilibrium point on the steady-state temperature map, thus, regulating the combustion timing during the fuel step changes.

is developed using the full-order model in [7]. Figs. 7 and 8 allow a comparison of the controlled performance with the observer-based feedback controller and a static feedforward controller during fuel steps 9–11–9 mg/cycle. Fig. 7 shows that the transient IVC temperature excursion is larger during the instantaneous step change in RBL commanded by the static feedforward controller, resulting in large excursion in the combustion phasing θ_{CA50}. The observer-based feedback controller, on the other hand, improves the combustion timing regulation during transients by slowing the RBL signal. The combustion timing θ_{CA50} converges to the desired value within 3 to 4 cycles.

Fig. 8 shows the load transitions 9–11–9 mg/cycle in the $T_{\rm er}-T_{\rm ivc}$ coordinates, where the interaction of these two temperatures determines the temperature dynamics of the HCCI engine [12]. The two solid nonlinear curves in Fig. 8 (similar to Fig. 10 in [12]) correspond to the steady-state characteristics of exhaust runner temperature $T_{\rm er}$ versus temperature at IVC $T_{\rm ivc}$ for fuel flow rate at 9 and 11 mg/cycle based on (56)–(69) and (45). As expected, the exhaust temperature increases and, thus, the curve shifts upward when the fuel flow rate increases. This nonlinearity associated with (56)–(69) introduces multiple equilibria to the temperature dynamics (9) with stable and unstable equilibria reported in [12]. The observer-based feedback controller stabilizes the system by explicitly taking into account the nonlinearity introduced by the function $f_c(T_{\rm ivc})$ in the temperature dynamics (9). Also, note that the nonmonotonic behavior shown in Fig. 8 indicates that there is a fuel-optimum $T_{\rm ivc}^*$ for which most of the chemical energy of the fuel is converted to useful mechanical work and not exhaust gas heat (low $T_{\rm er}$). In other words, temperature $T_{\rm ivc}$ determines combustion timing in the HCCI engine and affects the thermal efficiency. The temperature trajectories in Fig. 8 suggest that both controllers are able to regulate the steady-state IVC temperature $T_{\rm ivc}$ to the optimum equilibrium point $T_{\rm ivc}^*$ and associated combustion timing, while the observer-based feedback controller maintains tighter regulation during the fuel step changes.

Fig. 9 compares the performance with the observer-based feedback and static feedforward controllers during larger fuel steps (9–16–9 mg/cycle). In this condition, the performance with the static feedforward controller deteriorates substantially. First, while fueling level increases from 9 to 16 mg/cycle, the static feedforward controller causes a large temperature excursion and, thus, unhealthy combustion timing. When fuel increases, the static feedforward controller issues a command to decrease RBL immediately. During the simultaneous decrease in RBL, extremely late combustion or misfire occurs due to the dramatic drop in $T_{\rm ivc}$. Second, the engine temperature grows unbounded when fuel steps down from 16 to 9 mg/cycle. When fuel steps down, the static feedforward controller causes RBL to increase immediately, bringing into the cylinder a large

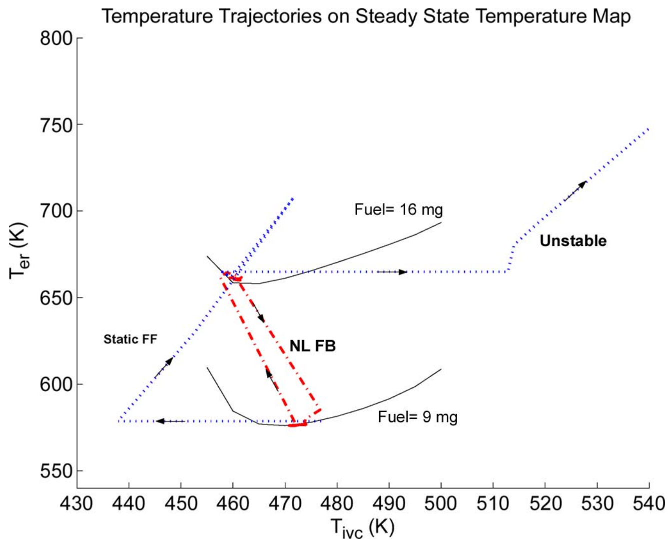

Fig. 9. Controlled temperature trajectories with the observer-based feedback controller and a static feedforward controller during fuel steps 9–16–9 mg/cycle. With the static feedforward controller, extremely late combustion timing occurs in the first cycle while fuel steps up and the engine temperature grows unbounded when fuel steps down.

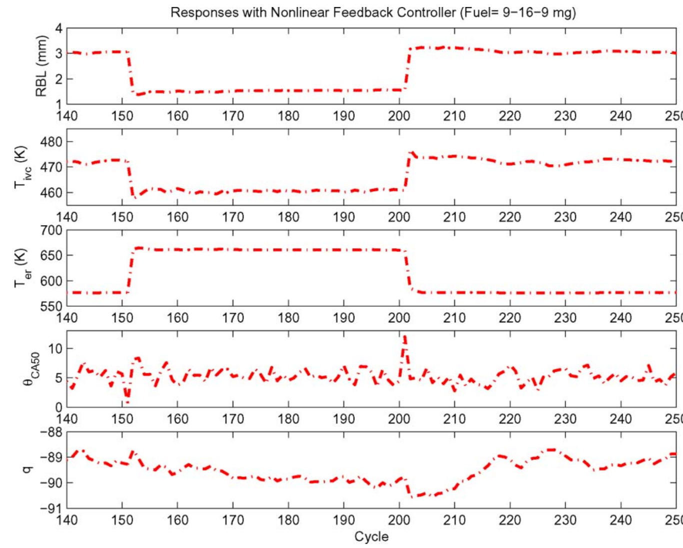

Fig. 10. Controlled responses with the observer-based feedback controller during fuel steps 9–16–9 mg/cycle.

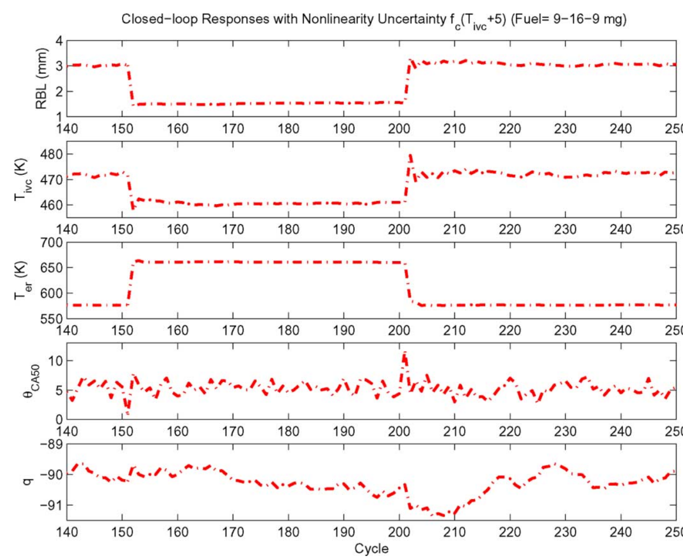

Fig. 11. Controlled responses with the observer-based feedback controller during fuel steps 9–16–9 mg/cycle with nonlinearity uncertainty $f_c(T_{\rm ivc}+5)$.

amount of hot exhaust gas that was produced in the previous cycle by the high fueling level (16 mg/cycle). The hot charge advances the combustion timing, causing the exhaust gas to become even hotter, which further advances the timing in the subsequent cycle. As can be seen in Fig. 9, the hot charge brings the temperature trajectory to the unstable region, as we observed in [12]. The observer-based feedback controller, on the other hand, is able to stabilize the temperature dynamics and achieve desired combustion timing during the load transition.

Fig. 10 shows the closed-loop responses with the observer-based feedback controller during fuel steps 9–16–9 mg/cycle. The combustion timing θ_{CA50} converges to the desired value within five cycles when fuel steps up. On the other hand, late combustion timing is observed during the first cycle when fuel steps down, but the observer-based feedback controller manages to stabilize the temperature dynamics and drive θ_{CA50} back to the desired value within two cycles. In [23], Santoso *et al.* observe from experiment that intermediate steps (valve profiles) are required for a successful transition from SI to HCCI. In other words, the control input needs to be filtered for a stable transition from high to low load as indicated by the results in Fig. 9. The observer-based feedback controller proposed in this paper slows down the control input to stabilize the cycle-to-cycle temperature dynamics.

The simulation results in Figs. 6–10 demonstrate that the nonlinear feedback controller (23), along with the observer (36), achieves good regulation of θ_{CA50} when applied to the full-order model in [7] despite the following:

1) neglecting the manifold filling dynamics (39)–(44);
2) approximating the exhaust runner heat transfer in (45) with the simple relation in (3);
3) approximating the nonlinear θ_{CA50} versus $T_{\rm ivc}$ relationship shown in Fig. 5 with a straight line (11).

Simulations also indicate that the observer-based feedback controller is robust to uncertainty in the temperature nonlinearity $f_c(T_{\rm ivc})$ in (9). This nonlinearity is critical for closed-loop stability and performance since it is included in the denominator of the feedback control law (23) and in the observer (36). To investigate the robustness of the observer-based controller against the uncertainty in this nonlinearity, instead of using the correct model (8) in the controller and observer, we shift the nonlinear function $f_c(T_{\rm ivc})$ along the $T_{\rm ivc}$ axis by a nonzero constant δ

$$T_{\rm bd} = f_c(T_{\rm ivc}+\delta, m_f) \tag{38}$$

which results in a shift of the solid nonlinear curve in Figs. 8 and 9 by δ along the $T_{\rm ivc}$ axis. With the shift introduced by the uncertainty δ, the controller cannot achieve perfect cancellation of the nonlinearity in the temperature dynamics and the observer cannot precisely estimate the state $T_{\rm ivc}$. Fig. 11 shows that the observer-based feedback controller is still able to regulate timing θ_{CA50} during the critical load transitions 9–16–9 mg

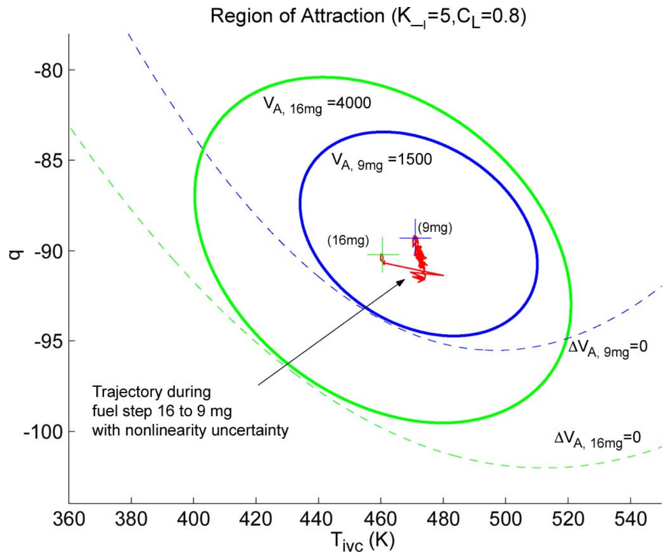

Fig. 12. Contours of $\Delta V_A(x) = 0$ (dashed line) and $V_A(x) = c$ (solid line) for fueling level 9 and 16 mg/cycle. Trajectory of the states with the observer-based feedback controller during fuel step 16-9 mg/cycle stays well inside the region of attraction $\{V_A(x) \leq c\}$.

with the uncertainty $\delta = 5$, even though a more oscillatory $T_{\rm ivc}$ and, thus, θ_{CA50} is observed during the first few cycles when fuel steps down from 16 to 9 mg. In short, the observer-based feedback controller does have a certain degree of robustness against uncertainty in the nonlinearity, as shown through the simulation. The oscillatory simulation results also imply the importance of modeling the $T_{\rm ivc} - T_{\rm er}$ temperature nonlinearity especially when operating points near the bottom of the curve are desired.

Fig. 12 shows the estimate of the region of attraction at fueling level 9 and 16 mg based on the analysis in Section IV. The region above each dashed curve in Fig. 12 represents the domain $D = \{x | \Delta V_A(x) < 0\}$ defined by (32) with the parameters a_0, a_1, and a_2 being functions of fueling level only for the selected c_L and K_I. For $c_L = 0.8$ and $K_I = 5$ K, $a_0(9\,\text{mg}) = 0.1764$, $a_1(9\,\text{mg}) = 0.011$ K^{-1} and $a_2(9\,\text{mg}) = -2.224 \cdot 10^{-4}$ K^{-2}. The region of attraction for each fueling level is then estimated by plotting the contour of $V_A(x) = x^T P x = c$ for increasing values of c until we determine the largest c for which $V_A(x) = c$ will be in D, the area above each dashed curve. The contours of $V_A(x) = c$ for the largest c at fueling level 9 and 16 mg are shown as the two solid ellipses in Fig. 12. Note that the region of attraction (the ellipse) expands as the fueling level increases. This phenomenon is explained as follows. As can be seen from (7) and (4), at a higher fueling level, the combustion duration becomes shorter and the exhaust temperature hotter. Therefore, a late start of combustion timing $\theta_{\rm soc}$ is required to regulate the timing when 50% of the fuel is burned (θ_{CA50}) and to stabilize the temperature dynamics by decreasing the temperature at IVC $T_{\rm ivc}$, as can be observed from (6). In other words, the operating point for a higher fueling level is farther from the point where higher $T_{\rm ivc}$ causes higher $T_{\rm er}$ in the nonlinearity of Fig. 9. Note also from Fig. 12, that the operating points for 9 and 16 mg are located well inside the smaller ellipse (attraction region of the equilibrium point at 9 mg). As a matter of fact, all the operating points from 9 to 16 mg are located well inside the attraction region of the equilibrium at 9 mg. As a result, the closed-loop trajectory of the critical load transition (fuel steps down from 16 mg to 9 mg) with the nonlinearity uncertainty $\delta = 5$ considered in Fig. 11, is able to stay within the region of attraction and with a safe margin from the boundary as shown in Fig. 12. This result implies that the controller is robust to additional uncertainties that are not considered in the simulations.

VII. Conclusion

An observer-based feedback controller for regulating combustion timing during load transitions is presented in this paper. The nonlinear feedback controller is based on a positive semidefinite Lyapunov function using a simplified control model which contains only the cycle-to-cycle temperature dynamics. A nonlinear observer for the state $T_{\rm ivc}$ is designed based on linearization of the error dynamics using output injection. The performance of the closed-loop system is evaluated via simulation of the full-order model in [7], which includes the manifold filling dynamics, exhaust runner heat transfer, combustion, and cycle-to-cycle variation of the combustion timing θ_{CA50}. The nonlinear feedback controller, along with the nonlinear observer, is able to regulate timing θ_{CA50} during the load transitions by reducing temperature excursions. Simulations and estimates of the region of attraction show that the designed controller is robust to uncertainties such as the manifold filling dynamics, exhaust runner heat transfer, the cycle-to-cycle variation of θ_{CA50}, and the uncertainty in the nonlinearity of the temperature dynamics. It is, however, also shown that the performance deteriorates when the nonlinear temperature dynamics are not well known. A nonoptimized controller such as a static feedforward controller can cause instability during a transition from a hotter region (higher fueling level) to a cooler region (lower fueling level). This is the same problem that needs to be solved while doing mode transition from SI to HCCI [23] or from CI to HCCI [24]. The control input needs to be filtered for a stable transition from a high to a low load by taking into account the cycle-to-cycle temperature dynamics. This is achieved by the nonlinear feedback controller designed in this paper.

Appendix

State equations

$$\frac{d}{dt}p_1 = \frac{RT_1}{V_1}(W_{01} - W_{1c}) \tag{39}$$

$$\frac{d}{dt}m_2 = W_{c2} - W_{20} - W_{2c} \tag{40}$$

$$\frac{d}{dt}b_2 = \frac{W_{c2}(b_{\rm er} - b_2)}{m_2} \tag{41}$$

$$\frac{d}{dt}p_2 = \frac{\gamma R}{V_2}\left(W_{c2}T_{\rm er} - (W_{20} + W_{2c})T_2\right) - \frac{(\gamma - 1)A_2 h_2}{V_2}(T_2 - T_w) \tag{42}$$

$$W_{c2}(t + \tau) = W_{1c}(t) + W_f(t) + W_{2c}(t) \tag{43}$$

$$b_{\rm er}(t + \tau) = b_{\rm bd}(t) \quad \text{where } \tau = N/120 \tag{44}$$

$$T_{\rm er}(t + \tau) = \frac{T_w T_{\rm bd}(t)}{(1 - \alpha_{ht})T_{\rm bd}(t) + \alpha_{ht} T_w} \tag{45}$$

where

$$\alpha_{ht} = \exp\left(\frac{-4h_{\rm er}RT_w}{C_pD_{\rm er}p_2}t_r\right)$$

which is derived by integrating the exhaust runner temperature dynamics from EVC to the middle of the intake stroke (t_r)

$$\frac{d}{dt}T_{\rm er} = -\frac{A_{\rm er}h_{\rm er}}{C_pm_{\rm er}}(T_{\rm er}-T_w),\ T_{\rm er}(0) = T_{\rm bd}(t-\tau)$$

with

$$m_{\rm er} = \frac{p_2V_{\rm er}}{RT_{\rm er}}$$

and

$$A_{\rm er} = 4V_{\rm er}/D_{\rm er}.$$

Conditions at IVC

$$W_{2c} = \frac{1}{\tau T_{\rm er}}\left(\kappa_0+\kappa_1\frac{p_1}{p_2}\right)\mathrm{RBL}^{\alpha} \quad (46)$$

$$W_{1c} \approx \frac{p_1V_{\rm BDC}}{RT_1\tau} - \frac{T_{\rm er}}{T_1}W_{2c} \quad (47)$$

$$p_{\rm ivc} = \beta_0+\beta_1p_1 \quad (48)$$

$$m_c = \frac{p_{\rm ivc}V_{\rm ivc}}{RT_{\rm ivc}} \quad (49)$$

$$x_r = W_2c\tau/m_c \quad (50)$$

$$T_{\rm ivc} = (1-x_r)T_1+x_rT_{\rm er} \quad (51)$$

$$b_c = (1-x_r)\frac{W_{1c}}{W_{1c}+W_f}b_1+x_rb_{\rm er} \quad (52)$$

$$b_{\rm bd} = \frac{\mathrm{AFR}_s+1}{\mathrm{AFR}_c+1}(1-b_c)+b_c \quad (53)$$

$$\mathrm{AFR}_c = [(1-b_1)W_{1c}+(1-b_{\rm er})W_{2c}]/W_f \quad (54)$$

$$\mathrm{AFR}_2 = (1-b_2+\mathrm{AFR}_s)/b_2. \quad (55)$$

From IVC to blowdown

$$\int_{\theta_{\rm ivc}}^{\theta_{\rm soc}} Ap_{\rm ivc}^n v_{\rm ivc}^{n_cn}(\vartheta)\exp\left(-\frac{E_av_{\rm ivc}^{1-n_c}(\vartheta)}{RT_{\rm ivc}}\right)d\vartheta = 1 \quad (56)$$

where

$$v_x(\vartheta_y) = V_c(\vartheta_x)/V_c(\vartheta_y) \quad (57)$$

$$\theta_{\rm soc} = \theta_{CA01} \quad (58)$$

$$T_{\rm soc} = T_{\rm ivc}v_{\rm ivc}^{(n_c-1)}(\theta_{\rm soc}) \quad (59)$$

$$\Delta\theta = k(T_{\rm soc})^{(-2/3)}(T_m)^{1/3}\exp\left(\frac{E_c}{3R_uT_m}\right) \quad (60)$$

where

$$T_m = T_{\rm soc}+e\Delta T \quad (61)$$

$$\Delta T = \frac{Q_{\rm LHV}m_f}{C_vm_c} \quad (62)$$

$$e = b_0+b_1\theta_{\rm soc}+b_2\theta_{\rm soc}^2 \quad (63)$$

$$\theta_{CA50} = \theta_{\rm soc}+.55\Delta\theta \quad (64)$$

$$\theta_c = \theta_{CA90} = \theta_{\rm soc}+\Delta\theta \quad (65)$$

$$T_{bc} = T_{\rm ivc}v_{\rm ivc}^{(n_c-1)}(\theta_c)$$

$$p_{bc} = p_{\rm ivc}v_{\rm ivc}^{n_c}(\theta_c) \quad (66)$$

$$T_{ac} = T_{bc}+\Delta T$$

$$p_{ac} = p_{bc}T_{ac}/T_{bc} \quad (67)$$

$$T_{\rm evo} = T_{ac}v_c^{(n_e-1)}(\theta_{\rm evo})$$

$$p_{\rm evo} = p_{ac}v_c^{n_e}(\theta_{\rm evo}) \quad (68)$$

$$T_{\rm bd} = T_{\rm evo}(p_2/p_{\rm evo})^{(n_e-1)/n_e}. \quad (69)$$

ACKNOWLEDGMENT

The authors would like to thank Prof. J. W. Grizzle from University of Michigan for fruitful discussions.

REFERENCES

[1] J. O. Olsson, P. Tunestal, B. Johansson, S. Fiveland, R. Agama, M. Willi, and D. Assanis, “Compression ratio influence on maximum load of a natural gas fueled HCCI engine,” SAE Int., Warrendale, PA, 2002-01-0111, 2002.

[2] D. S. Stanglmaier and E. Roberts, “Homogenous charge compression ignition (HCCI): Benefits, compromises, and future engine applications,” SAE Int., Warrendale, PA, 1999-01-3682, 1999.

[3] P. Najt and D. Foster, “Compression-ignited homegeneous charge combustion,” SAE Int., Warrendale, PA, 830264, 1983.

[4] R. H. Thring, “Homegeneous-charge compression-ignition (HCCI) engines,” SAE Int., Warrendale, PA, 892068, 1989.

[5] C. J. Chiang and A. G. Stefanopoulou, “Sensitivity analysis of combustion timing and duration of homogeneous charge cmpression ignition (HCCI) engines,” in *Proc. Amer. Control Conf.*, 2006, pp. 1857–1862.

[6] J. Martinez-Frias, S. M. Aceves, D. Flowers, J. R. Smith, and R. Dibble, “HCCI control by thermal management,” SAE Int., Warrendale, PA, 2000-01-2869, 2000.

[7] D. J. Rausen, A. G. Stefanopoulou, J.-M. Kang, J. A. Eng, and T.-W. Kuo, “A mean-value model for control of homogeneous charge compression ignition (HCCI) engines,” *ASME J. Dyn. Syst., Meas. Control*, vol. 127, no. 3, pp. 355–362, 2005.

[8] G. Shaver, J. Gerdes, P. Jain, P. Caton, and C. Edwards, “Dynamic modeling of residual-affected hcci engines with variable valve actuation,” *ASME J. Dyn. Syst., Meas. Control*, vol. 127, no. 3, pp. 374–381, 2005.

[9] C. J. Chiang and A. G. Stefanopoulou, “Control of thermal ignition in gasoline engines,” in *Proc. Amer. Control Conf.*, 2005, pp. 3847–3852.

[10] G. Shaver, M. Roelle, and J. Gerdes, “Decoupled control of combustion timing and work output in residual-affected HCCI engines,” in *Proc. Amer. Control Conf.*, 2005, pp. 3871–3876.

[11] J. Bengtsson, P. Strandh, R. Johansson, P. Tunestál, and B. Johansson, “Multi-output control of a heavy duty HCCI engine using variable valve actuation and model predictive control,” SAE Int., Warrendale, PA, 2006-01-0873, 2006.

[12] C. J. Chiang and A. G. Stefanopoulou, “Stability analysis in homogeneous charge compression ignition (HCCI) engines with high dilution,” *IEEE Trans. Control Syst. Technol.*, vol. 15, no. 2, pp. 209–219, Mar. 2007.

[13] J. B. Heywood, *Internal Combustion Engine Fundamentals*. New York: McGraw-Hill, 1988.

[14] J. C. Livengood and P. C. Wu, “Correlation of autoignition phenomena in internal combustion engines and rapid compression machines,” in *Proc. 5th Int. Symp. Combustion*, 1955, pp. 347–356.

[15] R. J. Tabaczynski, C. R. Ferguson, and K. Radhakrishnan, “A Turbulent entrainment model for spark-ignition engine combustion,” SAE Int., Warrendale, PA, 770647, 1977.

[16] J. Grizzle and J.-M. Kang, “Discrete-time control design with positive semi-definite lyapunov functions,” *Syst. Control Lett.*, vol. 43, pp. 287–292, 2001.

[17] A. Iggidr, B. Kalitine, and R. Outbib, “Semidefinite lyapunov functions stability and stabilization,” *Syst. Control Lett.*, vol. 9, pp. 95–106, 1996.

[18] R. Sepulture, M. Janković, and P. V. Kokotović, *Constructive Nonlinear Control*. Berlin, Germany: Springer, 1997.

[19] V. Lakshmikantham and D. Trigiate, *Theory of Difference Equation: Numerical Methods and Applications*. New York: Academic, 1988.

[20] H. K. Khalil, *Nonlinear Systems*. Englewood Cliffs, NJ: Prentice-Hall, 1996.

[21] K. Ogata, *Discrete-Time Control Systems*. Englewood Cliffs, PA: Prentice-Hall, 1987.

[22] M. Xiao, N. Kazantzis, C. Kravaris, and A. J. Krener, "Nonlinear discrete-time observer design with linearizable error dynamics," *IEEE Trans. Autom. Control*, vol. 48, no. 4, pp. 622–626, Apr. 2003.

[23] H. Santoso, J. Matthews, and W. K. Cheng, "Managing SI/HCCI dual-mode engine operation," SAE Int., Warrendale, PA, 2005-01-0162, 2005.

[24] C. Musardo, B. Staccia, M. Shawn, Y. Guezennec, and G. Rizzoni, "Supervisory control for nox reduction of an HEV with a mixed-mode HCCI/CIDI engine," in *Proc. Amer. Control Conf.*, 2005, pp. 3877–3881.

Chia-Jui Chiang (S'07) received the B.S. degree from National Chung Hsing University, Taichung, Taiwan, R.O.C., in 1995, the M.S. degree from National Taiwan University of Science and Technology, Taipei, Taiwan, R.O.C., in 1997, both in mechanical engineering, and he is currently pursuing the Ph.D. degree in mechanical engineering from the University of Michigan, Ann Arbor.

His research interests include modeling, stability analysis, and control of power systems, especially automotive propulsion systems.

Mr. Chiang was a recipient of a Best Paper Award for the 2006 AVEC Symposium.

Anna G. Stefanopoulou (SM'05) received the Diploma from the National Technological University of Athens, Athens, Greece, in 1991, and the M.S. degree in naval architecture and marine engineering, the M.S. degree in electrical engineering and computer science, and the Ph.D. degree from the University of Michigan, Ann Arbor, in 1992, 1994, and 1996, respectively.

Currently, she is a Professor in the Department of Mechanical Engineering, University of Michigan. She was an Assistant Professor (1998–2000) at the University of California, Santa Barbara, and a Technical Specialist (1996–1997) at the Scientific Research Laboratories at Ford Motor Company, Dearborn, MI. Her current research interests include control of advanced internal combustion engines and fuel cell power systems.

Mrdjan Janković (F'04) received the Bachelor degree from the University of Belgrade, Yugoslavia, in 1986, and the Masters and Doctoral degrees from Washington University, St. Louis, MO, in 1989 and 1992, respectively.

He held a Postdoctoral Teaching and Research positions with Washington University and University of California, Santa Barbara. He joined Ford Research and Advanced Engineering Laboratory, Dearborn, MI, in 1995, where he is currently a Technical Leader in the Powertrain Controls Department. His research interests include automotive engine control, nonlinear control, and time-delay systems. He has coauthored *Constructive Nonlinear Control* (Springer-Verlag, 1997) and holds over 30 U.S. and European patents.

Dr. Janković served on the Editorial Board of the IEEE TRANSACTIONS ON CONTROL SYSTEMS TECHNOLOGY from 1997 to 2005. He was a recipient of the Ford Research Technical Achievement Award and two Best Paper Awards (IEEE TCST 2002 and AVEC 2006).